,

On the Very Low Frequency Scattering of Marine Propeller Noise by a Neighboring Cylinder

Elina Cros[*][1,2], Michel Roger[†][1], and Gilles Serre[‡][2]

[1]*Laboratoire de Mécanique des Fluides et d'Acoustique, UMR CNRS 5509, Ecole Centrale de Lyon, 69134 Ecully, France*

[2]*Naval Group Research, 199 avenue Pierre Gilles de Gennes, 83190 Ollioules, France*

The present work addresses the scattering of the tonal noise of a low-speed propeller by a rigid cylinder, both propeller and cylinder axes being parallel and at a short distance to each other, for which a compact regime is reached. The propeller and cylinder diameters are small compared to the acoustic wavelengths, as well as the propeller-cylinder distance. This arrangement is considered as a generic configuration of installed marine propellers. Only the dipole-like sources of the hydrodynamic noise of the propeller are considered, assuming rigid blades. The sound radiation from the propeller is formulated in two dimensions, for characteristic spinning modes of the tonal noise, based on the exact Green's function of the cylinder. The mode orders ± 1 are found the only efficient ones in free field. In the presence of the cylinder, all higher-order modes are scattered into the contrarotating mode -1 with a strong amplification, whereas they would not radiate in free field. A simple experiment, performed in air but with Helmholtz numbers typical of marine applications, confirms the generation of the mode -1 as a key behavior of the asymptotic Green's function of the cylinder. The results show that the installation effect is crucial for the analysis of marine propeller noise at very low frequencies. Cylinder scattering is also theoretically investigated for a pair of synchronized contra-rotating propellers. Basic differences between the non-compact and compact regimes characteristic of aeronautical and naval applications, respectively, are highlighted.

I. Introduction

The very-low frequency tonal noise is generally the most significant contribution to the total noise of marine propellers, for long-range propagation issues. As a key signature of ships, it is a matter of concern with regards to ship detection in defense applications, as well as to the protection of aquatic wild life. Therefore, the main involved mechanisms must be identified, and dedicated prediction models that could be introduced in optimization design loops must be developed.

The most crucial aspects of marine propeller noise are the so-called installation effects. Firstly, the propellers of marine vehicles are always mounted in the rear part of the ship hull, therefore they are partly embedded in a non-homogeneous and turbulent wake and/or interact with the turbulent boundary layer developing along the whole length of the hull. Random and periodic fluctuations are induced on the blades, leading to increased, respectively broadband and tonal, acoustic signatures. This first effect is referred to as the hydrodynamic installation effect : any deviation from a pure axisymmetric flow around the propeller axis produces noise. Secondly, the mounting of propellers in close vicinity of the hull makes the sound radiated from the blades scattered by the hull, in such a way that the radiating properties of the sources are strongly modified. This is especially pronounced for the sources of the tonal noise, known to result from the interference between isolated-blade contributions. As a result, the noise of an installed propeller can dramatically differ from what the free-field noise would be, even considering the same sources. This second effect is called the acoustic installation effect. Both installation effects are usually considered independently. The present work is focused on the second one, thus on the diffraction problem. In low Mach number compact configurations, the diffraction of volume-distributed sources by surfaces has been identified as a very efficient mechanism by, for instance, Crighton

---

[*]Phd candidate, Ecole Centrale de Lyon, elina.cros@ec-lyon.fr

[†]Professor, Ecole Centrale de Lyon, michel.roger@ec-lyon.fr

[‡]Research engineer, Naval Group, gilles.serre@naval-group.com
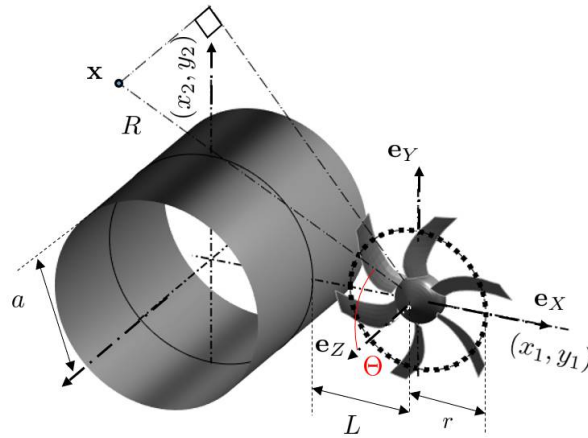
Fig. 1 Spherical coordinates for the three-dimensional formulation of rotor noise. Subsequent developments refer to the rotor-disk plane $(\mathbf{e}_X, \mathbf{e}_Y)$.

and Leppington [1], Doak [2], Howe [3], Curle [4] or Powell [5]. This is why marine propeller noise amplification is somehow expected when the installation is accounted for.

The noise radiated by a propeller is often predicted, relying on Ffowcs Williams & Hawking's formulation of the acoustic analogy [6, 7], which states that rotating blades can be replaced by equivalent sources in an ordinary wave equation. For free-field radiation, the equation is solved using the free-space Green's function. In the presence of surrounding surfaces, the wave equation (or the Helmholtz equation at specified frequencies) can be solved numerically with additional boundary conditions imposed on the surfaces, depending on the geometry. This has been the basis of hybrid methods developed in hydroacoustics to estimate the noise nearby the hull of a ship [8, 9] predicted with FEM (Finite-Element Method) or BEM (Boundary Element Method) simulations. Alternatively, a tailored Green's function can be used instead. For basic investigation of the scattering mechanism, a simplified geometry is chosen in this work, assimilating the ship hull, or some part of it, to a rigid cylinder. The exact cylinder Green's function for the Helmholtz equation is considered. This scope ensures analytical tractability and relevance of the results. The study is limited to propeller tonal noise, for which a clear modal structure, reminded in section II, can be defined.

At very low Mach numbers, the expected dominant sources are the lift fluctuations on the blades, acting as dipoles and responsible for the so-called unsteady-loading noise. This noise is essentially produced by the fluctuating hydrodynamic forces induced on the blades by cross-flow distortions. The distortions are not intrinsic features of the propeller: they depend on the installation. In a purely homogeneous axisymmetric flow, steady-loading noise and thickness noise would be the only remaining contributions, directly related to the design of the blades and the hydrodynamic performances. They should be negligible when compared to the unsteady-loading noise in the presence of a distortion, at least according to free-field criteria. The characteristic amplification associated with the asymptotic scattering by a compact obstacle leads to question this expectation and to reconsider the ranking of aforementioned mechanisms. This motivated the present research, dealing in particular with the impact of hull scattering on the steady-loading and thickness noise of installed marine propellers. In his formulation 1A, Farassat [10] shows that it is appropriate to describe thickness noise using Isom's developments [11]. Essentially, for any closed surface in arbitrary motion, the thickness noise is formally equal to the noise that would be radiated by a steady force of strength $\rho_o c_0^2$, where ρ_0 and c_0 are the density and sound speed of water. Furthermore, steady-loading noise and thickness noise have the same modal structure, made of rotor-locked modes. This allows to globally describe thickness noise and the complete loading noise by equivalent dipole sources. Therefore, only dipole sources are considered in the present work.

The amplification by compact scattering would be hard to evidence experimentally in water. In the present work, an experiment has been carried out in air, in an anechoic room of Ecole Centrale de Lyon, but with Helmholtz numbers representative of marine propellers conditions. The experiment is aimed at characterizing the scattered field, and at validating the analytical predictions. The paper is organised as follows. Some theoretical background on tonal rotating-blade noise for compact blades and the notion of associated source-modes are introduced in section II. The

2

experiment and accompanying model predictions are presented in section III, in a variable configuration associating a single propeller and a rigid cylinder. The exact cylinder Green's function is then used. The modeling approach is then extended to a pair of contra-rotating propellers in section IV, in order to assess basic scattering features for dual propulsion architectures.

II. Free-Field Tonal Noise Formulae

Elementary expressions of the tonal noise radiated by a propeller in the far field are first reviewed in this section. They are used only as a reference for the analysis of the modal properties of the radiated field. The formalism of source-modes is introduced as a complement, from which the sound field could be expressed uniformly in the whole space. Such a procedure is well suited when the near-field inspection is of some interest. It is also extendable to various configurations, such as a pair of synchronized propellers. The diffraction model is developed in a second step, based on the Green's function tailored to the geometry.

A. Rotating-Dipole Noise Formula

Only the tonal noise at harmonics of the Blade-Passing Frequency (BPF), caused by the steady-state hydrodynamics of the blades and by stationary azimuthal distortions, is considered in this work. In free field but with the real flow corresponding to an installed configuration, thus the true sound sources, this noise is predicted relying on Ffowcs Williams & Hawking's formulation of the acoustic analogy [6, 12]. The formulation is reduced to dipole source terms of arbitrary orientation, as stated in the introduction. The tonal noise is formulated here in the frequency domain and in the far-field, in a way suited to highlight modulation by the azimuthal flow distortions and interference properties between blades. A general expression for the far-field sound pressure radiated by a compact blade element and the similar ones on each blade, at the tone of angular frequency $\omega = \mu B \Omega$, where B is the number of blades and Ω the rotational frequency, can be written as (see for instance reference [13])

$$p_{\mu B}(\mathbf{x}) = \frac{\mathrm{i}\, k_{\mu B} B}{4\pi R} \mathrm{e}^{\mathrm{i}\, k_{\mu B} R} \sum_{s=-\infty}^{\infty} \mathrm{e}^{\mathrm{i}\,(\mu B - s)(\phi - \pi/2)} \times$$

$$\left[\mathrm{J}_{\mu B - s}(\mu B\, M\, \sin\Theta) \left(F_s^{\mathbf{A}} \cos\Theta - F_s^{\mathbf{T}} \frac{(\mu B - s)}{\mu B\, M} \right) \right.$$

$$\left. + \mathrm{i} F_s^{\mathbf{R}} \sin\Theta\, \mathrm{J}'_{\mu B - s}(\mu B\, M\, \sin\Theta) \right], \quad (1)$$

with the notations defined in Fig. 2, where $M = \Omega r/c_0$ is the tangential Mach number of the element and $k_{\mu B} = \mu B \Omega / c_0$ is the acoustic wavenumber. Each tone is expressed as a sum of spinning radiation modes. A mode is a diverging pressure wave combined with an azimuthally periodic pattern spinning at some phase speed, forced by the dipole source strength. $(F_s^{\mathbf{R}}, F_s^{\mathbf{T}}, F_s^{\mathbf{A}})$ are the Fourier coefficients of the blade force (**R,T,A**, denoting the force components in the radial, tangential and axial directions, respectively), referred to as the blade loading harmonics (BLH). Equation (1) is one way to analyze the far-field tonal noise of rotating machines, extensively used for fans and turbomachines in air.

In the plane of the rotor disk considered later on for two-dimensional studies, $\Theta = \pi/2$, the formula (1) is reduced to

$$p_{\mu B}(\mathbf{x}) = \frac{\mathrm{i}\, k_{\mu B} B}{4\pi R} \mathrm{e}^{\mathrm{i}\, k_{\mu B} R} \sum_{s=-\infty}^{\infty} \mathrm{e}^{\mathrm{i}(\phi - \pi/2)} \left[F_s^{\mathbf{T}} \frac{n\, \mathrm{J}_n(\mu B\, M)}{\mu B\, M} + \mathrm{i} F_s^{\mathbf{R}}\, \mathrm{J}'_n(\mu B\, M\, \sin\Theta) \right]. \quad (2)$$

It is valid in a three-dimensional space but will not be directly implemented as such in the following. For very low tangential Mach numbers $M = \Omega r/c_0 \ll 1$, the expression can still be simplified by considering the asymptotic expansions of the Bessel functions and of their derivatives for small arguments, not detailed here. The net result is that the modes of orders $n = \mu B - s$ such that $|n| \geq 2$ are negligible in the distant free field. The orders $n = \pm 1$ are the only contributing ones for the tangential force component and the orders $n = \pm 1$ and $n = 0$ the ones for the radial component.

B. Source Modes

The contribution of the near field terms is neglected in Eq. (1), whereas it is essential for installation-effect studies, as pointed out by, for instance, Roger *et al.* [14–16]. A more general form of Eq. (1) could be derived for this purpose. A dedicated approach based on the source-mode formalism is used instead in this paper. The sound field of the spinning

3
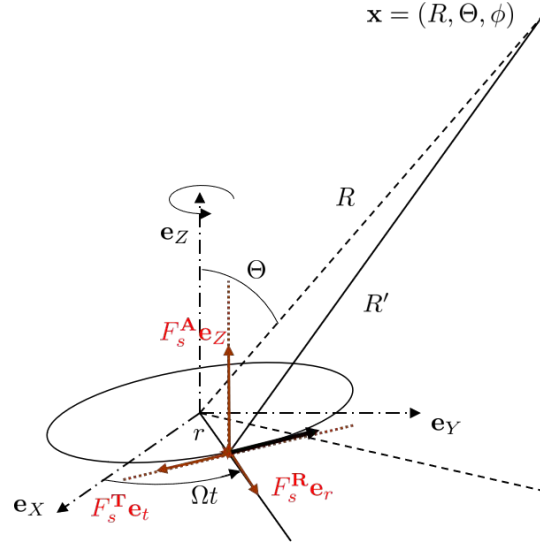
Fig. 2   Reference frame attached to a rotating dipole

.

radiation mode of order $n = \mu B - s$ for a compact blade element at a given radius r can be equivalently reproduced by a continuous circular distribution of stationary and phased dipoles at the same radius with constant amplitude F_s [17]. For the mode of order n associated with the BLH of order s, $F(\alpha, t) = F_s e^{-i \mu B \Omega t}$ where $F_s = F e^{i n \alpha}$ defines a spinning radiation mode of angular speed $\Omega_s = \mu B \Omega / (\mu B - s)$. For practical implementation, this circle distribution is discretized. As diffraction problems are usually formulated in the frequency domain for stationary sources, the scattering can be calculated for each point dipole of a source-mode circle. The total sound field of a propeller can always be reproduced by linear superposition. Such a procedure is well suited for the assessment of the scattering by obstacles of arbitrary shape. It holds for both two-dimensional and three-dimensional studies.

III. Installation Effects Caused by a Cylinder at Low Mach Number

This section investigates the radiated field of a single propeller placed close to a cylinder. It is aimed at highlighting the acoustic installation effect. The measurements are made in compact configurations representative of small-size cooling fans or of marine propellers. The experimental set up is detailed in a first step. In a second step, the measured sound power levels at the BPF are compared for free-field and installed configurations with various propeller-cylinder distances. A modal decomposition of the acoustic pressure field is performed, from simultaneous microphone-array measurements, in order to assess the modal content of the scattered field.

A. Experimental Setup

The experiment has been performed in an anechoic chamber of the ECL-LMFA (Laboratoire de Mécanique des Fluides et Acoustique of École Centrale de Lyon), the dimensions of which are $6\,\text{m} \times 5\,\text{m} \times 4\,\text{m}$. A three-bladed propeller of 65 mm diameter is mounted at one end of a cylindrical hub of diameter 27 mm and length 170 mm, as shown is Fig. 3. It is powered by a DC-motor inserted in the hub at the speed regime of 11800 rpm corresponding to a blade-tip Mach number of about 0.1. The scattering cylinder has a diameter of 60 mm and a length of about 1 m. The propeller plane is at mid-length. The hub is placed parallel to the scattering cylinder, its axis being at a distance L from the cylinder axis, as shown in Fig. 4. 12 microphones are regularly distributed on a circle of radius 1 m centered on the cylinder axis, surrounding both the propeller and the section of cylinder. The measurements are made in the rotational plane $(\mathbf{e}_X, \mathbf{e}_Y)$ as sketched in Fig. 4. The rotational speed corresponds to a BPF of 590 Hz.

The separation L can be varied by means of rods of 5 mm diameter, diametrically sliding through the cylinder. The minimum value is $L = 65$ mm. In this way, the characteristic Helmholtz numbers indicate that the distance between the cylinder and the sources, the radius of the cylinder and the radius of the source-modes are all much smaller than the acoustic wavelength. More precisely, these compactness conditions read $ka \ll 1$, $kr \ll 1$ and $kL \ll 1$ according to the

4

(a) Global view

(b) zoom on the propeller
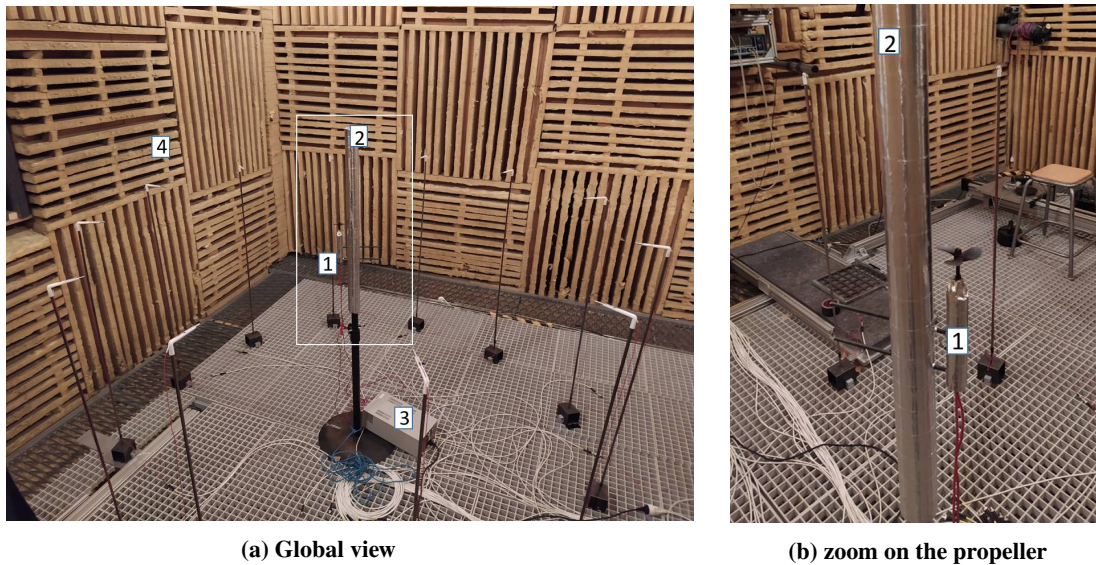
Fig. 3 View of the experimental setup: 1. 3-blades propeller, 2. Rigid cylinder, 3. Motor, 4. Microphones

notations in Fig. 1. The acoustically compact regime corresponds to marine applications but is also expected when considering the noise radiation from small cooling fans at a low rotational speed [18–20]. The present experiment is seen as a convenient way of reproducing the conditions of marine propellers at very low Mach number in air, from the point of view of characteristic Helmholtz numbers.
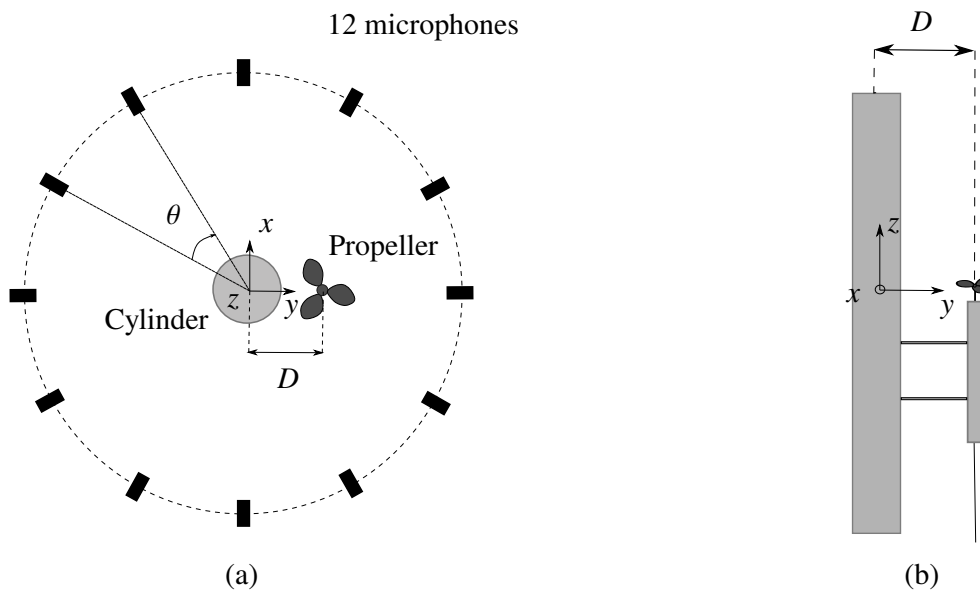
Fig. 4 Schematic of the experiment setup. (a): top view; (b): side view.

B. Data Analysis

Typical PSD (Power Spectral Densities) of the measured sound pressure are shown in Fig. 5 for the free-field and installed configurations. In the first case, the acoustic signature (red) is recorded with the isolated propeller mounted at the end of a vertical support, ensuring nearly-axisymmetric cross-flow. In the second case, because the propeller is close

5
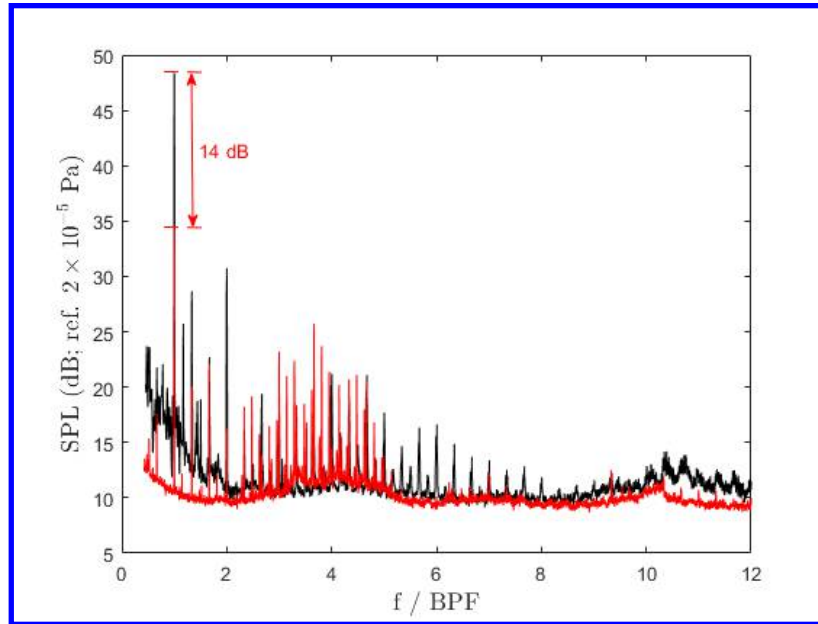
Fig. 5   Typical sound-pressure spectra for the propeller in free field (—) and installed (—) close to the cylinder. BPF = 590 Hz.

to the cylinder, additional flow distortions are not excluded; they have not been accurately measured. The key result is that the peak levels at the first BPF tones dramatically increase as the propeller is approached close to the cylinder. The increase at the first BPF is of 14 dB. It could result from either the aforementioned additional distortion, or the asymptotic scattering regime. This is why a modal analysis of the field at the first BPF has been performed for the two configurations, the instantaneous pressures measured by the circular array of microphones being expanded into spinning modes.

(a)

(b)
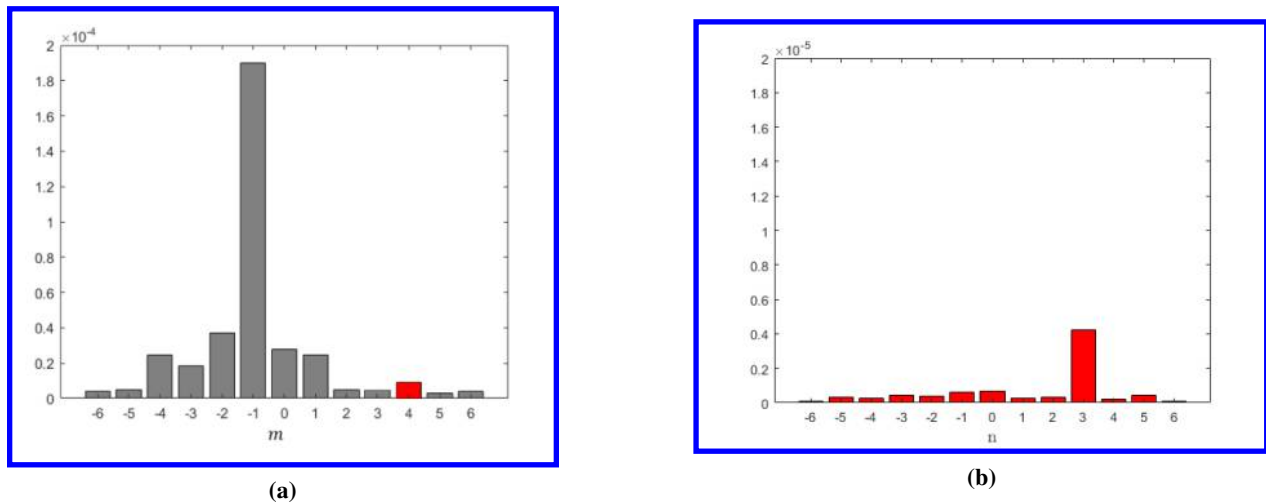
Fig. 6   Bar graphs of the amplitudes of the spinning-mode expansion for the first BPF. (a): installed propeller for the shortest propeller-cylinder distance (red bar reminding the dominant mode of subplot (b)). (b): zoom on the modal decomposition of the free-field with a different scale. Negligible values outside the harmonic range [-6; 6]. Same arbitrary scale on both plots.

Figure 6 illustrates bar graphs of the modal amplitudes at the first BPF, for the two configurations previously mentioned. Two key results are highlighted. Firstly, in Fig. 6b, the free-field modal content is found to be dominated by the

rotor-locked mode $n = 3$ corresponding to the number of blades. For this test, the propeller is placed at the center of the circle of microphones. The result is attributed to steady-loading and/or thickness noise, both having the same modal structure. It confirms that the free-field set-up is indeed free of significant residual azimuthal distortion. Once the propeller is displaced away from the array center as shown in Fig. 4-a, the mode 3 is seen mainly as the mode 4; this is emphasized by the small red bar in Fig. 6a. This effect of de-centering has been reproduced by a simple simulation of the modal expansion, not detailed here. Secondly, in Fig. 6a, the vicinity of the propeller to the cylinder corresponds to a totally different modal content, with the strong emergence of the mode $n = -1$. Furthermore, a much higher amplitude is produced than in free field. The amplification and its modal content suggest that the noise increase observed in Fig. 5 is not of aerodynamic origin. Indeed, the residual distortion is expected to generate low-order blade-loading harmonics, thus values of $n = \mu B - s$ rather between +1 and +5. The most important result is that the noise generated is dramatically amplified by the effect of the cylinder, with an unexpected conversion of the mode $n = +3$ into the mode order $n = -1$.

These outcomes have motivated particular theoretical considerations, based on the Green's function tailored to a rigid cylinder. The analytical approach, considered for separate publication, has highlighted that higher-order modes $n > 1$ are found to only generate evanescent waves in free field, whereas they experience a very strong amplification in the presence of the cylinder. The amplification generates the radiating mode of order -1, whatever the direct mode order n is, with inversion of the phase rotation. This is briefly reminded and illustrated in the following section.

C. Analytical Model of Propeller Tonal Noise Scattering by a Cylinder

An alternative to Green's formula when solving a problem of acoustics in the presence of solid boundaries is to consider a Green's function tailored to the geometry. In the present study, the sources are assumed very close to the surface of a rigid cylinder of circular cross-section. The tailored Green's function, G'_t, is determined by adding the free-field Green's function, G'_i, a second term, G'_s, such that the total Green's function $G'_t = G'_i + G'_s$ fulfills the rigid-wall boundary condition on the cylinder surface.
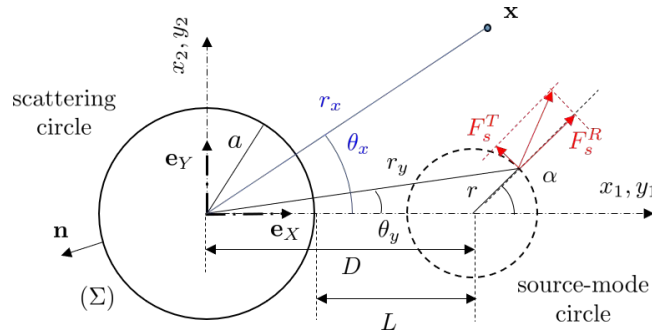
Fig. 7   Polar coordinates and main notations used in the present formulations.

In the present, preliminary two-dimensional analysis, the free-field Green's function with origin at the center of the circular cross-section, as sketched in Fig. 7 is used. If $\mathbf{x} = (r_x, \theta_x)$ and $\mathbf{y} = (r_y, \theta_y)$ stand for the observer and source points, respectively, it reads

$$G'_i(\mathbf{x}|\mathbf{y}, \omega) = \frac{\mathrm{i}}{4} k \, \mathrm{H}_1^{(1)}(k|\mathbf{x} - \mathbf{y}|) \, . \tag{3}$$

The presence of the cylinder of radius a is accounted for by the scattered part of the tailored Green's function, written as :

$$G'_s(\mathbf{x}|\mathbf{y}, \omega) = \frac{1}{4\mathrm{i}} \sum_{m=0}^{+\infty} \epsilon_m B_m \mathrm{H}_m^{(1)}(kr_y) \cos\left[m(\theta_y - \theta_x)\right] \, , \tag{4}$$

where $\epsilon_m = 1$ for $m = 0$ and $\epsilon_m = 2$ for $m > 0$, $k = \mu B\Omega/c_0$ being the acoustic wavenumber. The rigidity condition $\partial G'_t/\partial n = 0$ at $r_y = a$ yields :

$$B_0 = -\frac{\mathrm{J}_1(ka)}{\mathrm{H}_1^{(1)}(ka)} \, \mathrm{H}_0^{(1)}(kr_x) \, , \qquad B_m = -\frac{\mathrm{J}_{m-1}(ka) - \mathrm{J}_{m+1}(ka)}{\mathrm{H}_{m-1}^{(1)}(ka) - \mathrm{H}_{m+1}^{(1)}(ka)} \, \mathrm{H}_m^{(1)}(kr_x) \, , \, m \geq 1 \, ,$$

7

J_m and $\mathrm{H}_m^{(1)}$ being the Bessel and Hankel functions of order m and of the first kind. Performing this for all points of a discretized source mode and then summing linearly all contributions enables the synthesis of the complete radiated field of a source-mode, and by extension of an installed propeller close to a cylinder.

The exact two-dimensional Green's function for a cylinder is selected here to mimic the cylinder of the experiment, as a generic configuration. Once elucidated in this simple geometry, the mechanism of amplification is expected to also take place in other configurations as long as the regime is acoustically compact. The radiated sound pressure is expressed by the scalar product of the source-mode dipole strength by the first gradient of the Green's function with respect to the source coordinates:

$$\mathbf{F}_s \cdot \nabla(G_t') = \mathbf{F}_s \cdot \nabla(G_i' + G_s')$$

where $\mathbf{F}_s$ is the force vector and $F_s = F\,\mathrm{e}^{\mathrm{i}n\alpha}$ the dipole strength. The derivations of $\nabla(G_i' + G_s')$ are similar to those provided by Gloerfelt *et al.* [21].

The Helmholtz characteristic numbers of the experiment are $ka = 0.33 \ll 1$, $kr = 0.035 \ll 1$, $kL = 0.38 \ll 1$. In this way, the low Mach number is still quite too high but the Helmholtz numbers are similar to those of the tonal noise of a marine propeller. The result in Fig. (8a) illustrates the steady-loading noise of the $B = 3$ bladed-propeller at the first BPF ($\mu = 1$) in free-field using the analytical model. The mean force F_0 of the rotor is associated to the rotor-locked mode $n = \mu B$. The complete configuration involving the presence of a scattering cylinder is shown in Fig. (8b). Both representations are in the plane of the source circle. The arrow in Fig. (8a) stands for the source-mode phase rotation, representative of the steady-loading noise of a counterclockwise rotating propeller. The pressure fluctuations are concentrated close to the source circle but rapidly vanish away from it, as a consequence of the values of the Bessel function approaching zero in the formulation of section II. Once the source-mode is placed close to the scattering circle, the sound is reinforced and the modal structure is modified. Indeed, the total radiated field becomes very efficient by the effect of the compact Green's function, featuring a dramatic amplification. The wave-front pattern strongly differs; it exhibits one lobe spinning in the clockwise direction, indicated by the arrow in Fig. (8b). This behaviour confirms the aforementioned emergence of the mode order $n = -1$, observed in the experiment. The same result has been found valid also for all higher-order azimuthal modes, as reported by Cros *et al.* [22].

(a)　　　　　　　　　　　　　(b)
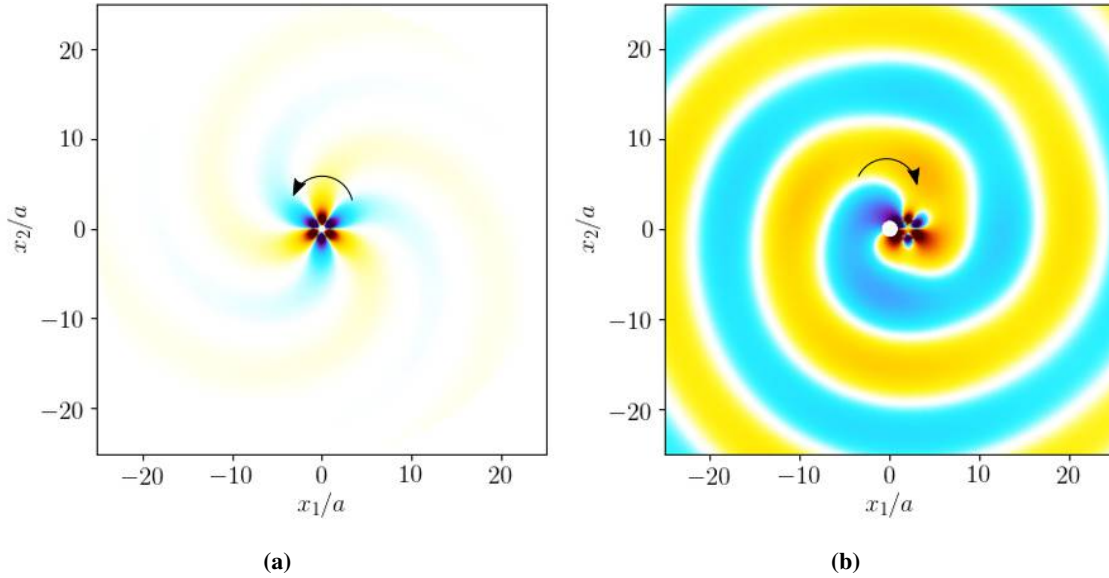
Fig. 8 Instantaneous pressure field of a circular array of phased dipoles in free-field (a) and in the presence of a scattering cylinder (b) for the rotor-locked mode $n = 3$ representative of the experiment. Comparable color scales.

A complementary study, including two contra-rotating propellers close to a cylinder, is addressed theoretically with the exact tailored Green's function in the next section, for two extreme configurations of compact and non-compact regimes. In fact, the formalism is valid for arbitrary values of the parameters, therefore it holds for aeronautic applications at high rotational speeds, as well as for rotating machines at low Mach Number. The comparison allows to highlight the specific features of marine applications.

IV. 2-D Scattering Model for a Pair of Contra-Rotating Propellers Near a Cylinder

Two specific aspects of a dual propulsion system made of side-by-side contra-rotating propellers are addressed in the present section, namely the synchronization of two circles of modal sources on the one hand, and their scattering by a neighboring cylinder on the other hand. Practically, the total scattered field is obtained by superimposing the fields of individual source modes. The study is aimed at assessing the interference between propellers and the properties of its combination with the scattering by the cylinder. Basic configurations related to aeronautical and naval applications are opposed to highlight the importance of the compactness regime on the diffraction. A similar approach has been detailed by M. Roger [17] in the investigation of combined propeller synchronisation and edge scattering.
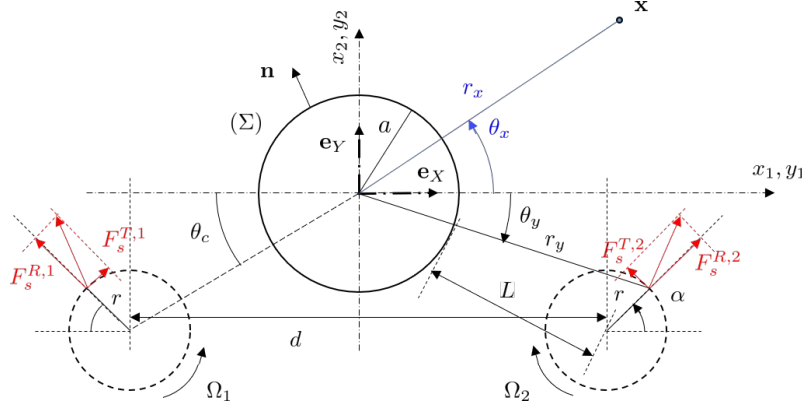
Fig. 9   Polar coordinates and main notations used for two source-modes.   Note the image-like definition of dipole strengths.

A. Synchronized Propellers in Free Field

The behavior of synchronized, side-by-side propellers in free field is detailed first, for a better understanding of diffraction aspects addressed in the next section. By linear superposition, the total sound field of two propellers can always be reconstructed by summing individual source-mode fields. It is worth reminding that the source-modes are forced by the steady-state hydro/aerodynamics and by azimuthal flow distortions, at the origin of the unsteady-loading noise. Each source-mode of order n is associated to either a BLH F_s with $s = \mu B - n$, or the steady-state force F_0 referring to the rotor-locked $n = \mu B$. This is illustrated by instantaneous sound-pressure patterns of a pair of contra-rotating modes at a single radius $r = R_0$, for naval and aeronautical configurations in Figs. 10 and 11, respectively. In absence of side-flow, but with possible distortions due, for instance, to the installation on a non-axisymmetric hub, it can be guessed that the distortion on one propeller is the symmetric image of the distortion on the other one. This is the case as well if the installation effect is caused by a symmetric shape, such as a ship hull or the fuselage of an airplane, with symmetrically installed propellers on both sides. As a result, the unsteady forces on the blades are also images of each other, as illustrated in Fig. 9 for zero propeller phasing (propellers synchronized in such a way that the blade tips are 'face to face' at their shortest distance). The same forces would be simply phase-shifted for a different phasing. Therefore, the same source-modes can be assumed as elementary waves for both propellers, but with some relative angular phase and with opposite phase speeds, noted Ω_1 and Ω_2 in the figure. In the test, the dipole axes are assumed tangent to the considered source-mode circles, thus with zero radial component, which is a reasonable assumption for an axial-flow propeller as long as blade sweep is neglected. Similar developments could be made for a radial component. The free field of one counterclockwise spinning mode taken as reference is depicted in Figs. 10a and 11b. The modes are phase-shifted by half a lobe, which leads to complete cancellation in the median plane. As an example, the result in Fig. 10a depicting the mode $n = 2$ mimics the unsteady-loading noise for a blade loading harmonic F_3 of a 5-bladed propeller ($B = 5$) at the first BPF ($\mu = 1$). The source frequency is $10\,\text{Hz}$. The size of the source circle is much smaller than the acoustic wavelength, which means that the configuration is acoustically compact, representative of marine propeller. The spiral wavefronts correspond to a moderate efficiency in this case. Because of the compactness the free-field pressure amplitude is found to decrease as the mode order increases for the same assumed dipole strength, and the only efficient mode is $n = 1$. The two mode sources are placed close to each other with the center-to-center distance $d = 5.7\,R_0$, with $R_0 = 1\,\text{m}$. Because they spin in opposite directions ($n = \pm 2$), the individual spiral wavefronts are

restructured in a standing-wave pattern with extinction angles, as seen in Fig. 10b. Globally, the synchronization exhibits a quadrupole-like pattern, with an overall pressure doubling. The main aspect of synchronized propellers in compact configuration is that the resulting standing wave has a number of lobes equal to the mode order, for any source-mode.

(a)　　　　　　　　　　　　　　　　**(b)**
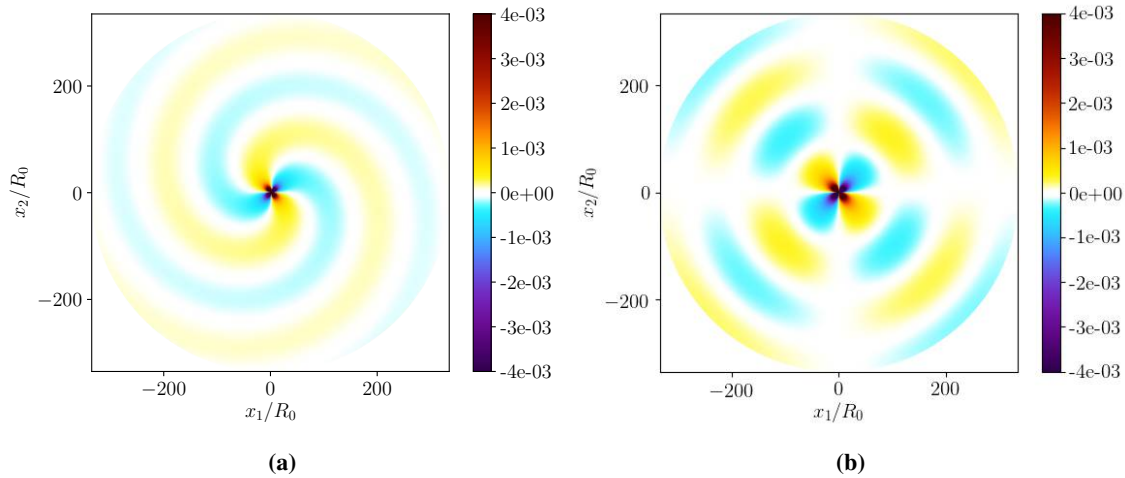
Fig. 10　Instantaneous free-field pressure patterns for the counterclockwise source mode $n = 2$ (a) and for the pair of contra-rotating source modes $n = \pm 2$ (b) in compact configuration. Circle radius $r = R_0 = 1$ m, and center-to-center distance $d = 5.7\,R_0$, frequency 10 Hz and blades number $B = 5$. Note that the cylinder and source circle cannot be seen because of their small sizes compared to the wavelength. Sound speed 1500 m/s.

(a)　　　　　　　　　　　　　　　　**(b)**
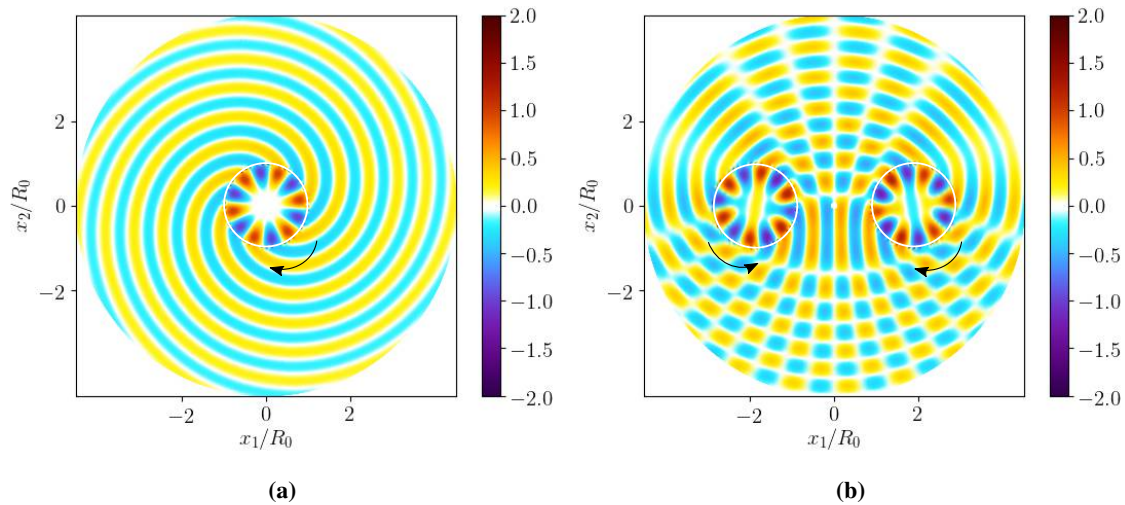
Fig. 11　Instantaneous free-field pressure patterns for the counterclockwise source mode $n = 6$ (a) and for the pair of contra-rotating source modes $n = \pm 6$ (b) in non-compact configuration. Circle radius $r = R_0 = 1$ m, center-to-center distance $d = 2.5\,R_0$, frequency 600 Hz, blades number $B = 10$. Sound speed 340 m/s.

The non-compact configuration in Figs 11, at the higher BPF frequency 600 Hz, exhibits totally different features. It corresponds to a 10-bladed propeller of radius $R_0 = 1$ m. Though considering simplifications as the study in two-dimensional and the significant advancing-flight speed neglected, the configuration is believed representative of an aeronautical propeller. The instantaneous pressure of the isolated mode $n = 6$ is depicted in Fig. 11a, and the modes $n = \pm 6$ are plotted in Fig. 11b for a separation $d = 3.5\,R_0$. The sources-circle are substantially larger than the wavelength in this case. The wavefronts spinning in the counterclockwise direction are clearly identified, with a rather progressive attenuation imposed by the cylindrical spreading. When the source-modes interact in Fig. 11b, interference fringes are produced in the lower part of the map because the spiral wavefronts emitted from both propellers propagate against

each other. In the upper part, they propagate away from each other. Typically, four extinction angles are found with the present phasing. The same configurations are assessed below, in the presence of a scattering cylinder.

B. Cylinder Scattering of Two Modal sources

1. Definition of the Test Case

The pairs of contra-rotating propellers previously considered in free field in Figs. 10 and 11 are now addressed close to a scattering cylinder. The scattering is calculated analytically from Eq-4 in order to assess basic features. At very low frequency, the scattering by a cylinder of one propeller showed amplification, associated with the generation of the radiating mode $n = -1$, whatever the mode order $n > 1$ is. But the interference of two propellers possibly modifies the scattering behavior, which motivates a dedicated inspection. The study is again performed also for the non-compact configuration typical of aeronautic applications. The sources-modes, of radius $r = R_0$, are located at a distance L from the surface of the cylinder of radius a. Their centers are located at angle $\theta_c = -\pi/4$ below the x-axis. In the two cases, the two source-modes are very close to the cylinder and contra-rotating, as indicated by the arrows in Fig.-12. The notations are summarized in Fig.-9. Test-case results obtained with the exact analytical model are shown in Figs. 12, 13 and 14 depicting the instantaneous-pressure maps for the two configurations.

2. High-Frequency Test case

The first case is dedicated to aeronautical application. The two synchronized propellers depicted in Fig. 11b in free field, are now placed close to the scattering circle of radius $a = 1.5\,\text{m}$. The resulting instantaneous pressure field is plotted in Fig. 12.
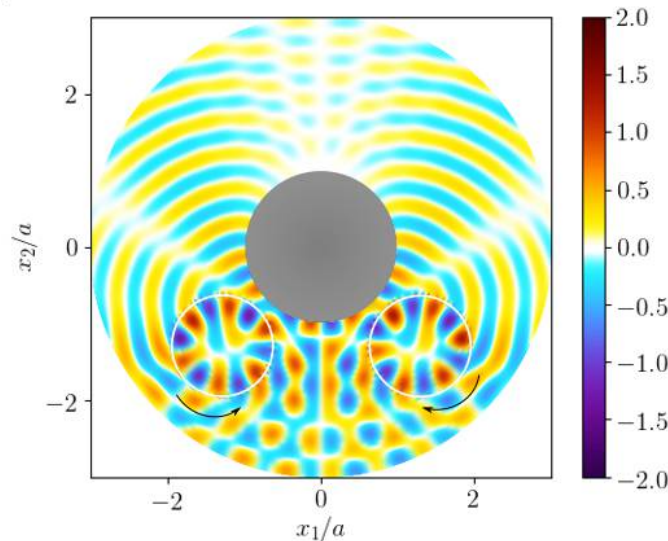
Fig. 12   Instantaneous pressure maps for the pair of contra-rotating source-modes in the presence of a scattering cylinder, for the modes $n = \pm 6$. Frequency 600 Hz, center-to-center distance $d = 5.7\,R_0$ with $R_0 = 1\,\text{m}$. Distance between cylinder axis and source-circle axis $L = 1.25\,\text{m}$. Circles located at $\theta_c = -\pi/4$ below the horizontal axis. Sound speed $c_0 = 340\,\text{m/s}$.

The grey disk corresponds to the scattering cylinder, and the two source-modes are featured by white circles. The source-mode radius and the cylinder are substantially larger than the wavelength in this highly non-compact case. When the cylinder is present, the incident wave coming from the two propellers is distorted. The n direct spiral wave-fronts are distorted when approaching the cylinder, forced to stay locally normal to the surface by the rigid-wall boundary condition (zero normal derivative). The interference fringes observed in free-field are reinforced and distorted on the lower part of the map because of the combined contributions of the scattered and direct fields. The four extinction angles in the upper part noticed in free field in Fig 11b are now replaced by a shadow zone on the top of the cylinder. This behavior is similar to the creeping waves which develop in the theory of diffraction, as waves travel around curved

11

obstacles towards the shadow zone. In this non-compact regime, the scattering redefines the directivity of outgoing waves, but the order of magnitude of the total radiated power remains the same. No amplification is expected, unlike in the compact case described in the next section.

3. Low-Frequency Test Case

The Helmholtz numbers of the test are $kR_0 = 0.034$, $ka = 0.10$ and $kL = 0.034$. The maps of instantaneous pressure for the pairs of contra-rotating source-modes $n = \pm2$ and $n = \pm3$ and for the installed configuration are shown in Figs. 13 and 14, respectively, for two values of the source-to-cylinder distance. In both figures, the cylinder, of radius $a = 3$ m is indistinguishable because of the much larger acoustic wavelength. In particular, the free field of the source-modes $n = \pm2$ described in Fig. 10b must be compared to the total scattered field in Fig. 13. A zero-phasing synchronization is imposed for the source-modes $n = \pm3$ reported in Fig. 14, whereas the half-lobe phasing is imposed for the case $n = \pm2$. This corresponds to an equivalent perfectly symmetric image, with a local maximum in the median plane, instead of a zero sound field. In both cases, the total field is considerably higher than the free field for the shortest investigated distance to the cylinder in Figs. 13a and 14a. The amplification is due to the effect of the compact Green's function, as observed for isolated modes in Section III. It must be noted that the free field of the source modes $n = \pm3$ is not plotted here because it is evanescent, much lower than for the modes $n = \pm2$. This means that the total field is definitely dominated by the scattered field alone. In fact, it could be observed that the scattered field decays proportionally to the factor $e^{r_x \sqrt{(n/R_0)^2 - k^2}}$.

Another major difference is that the total field exhibits dipole-like patterns for mode orders $n > 1$, whereas the free field of the mode $n = \pm2$ was found to produce a quadrupole-like pattern. The equivalent dipole is a common feature of all pairs of contra-rotating modes in the asymptotic regime, whatever the mode order is, as a consequence of the associated emergence of the mode ±1. The orientation of the dipole is a matter of phasing between the two modes. The configuration of modes $n = \pm3$ in Fig 14 corresponds to a main radiation along the vertical axis. For the modes $n = \pm2$ in Fig 13, the dipole axis is along the horizontal axis. This simple property might have important applications in marine propulsion systems, were the propellers installed on both sides of a hull synchronized accordingly. Indeed, the free surface of the water is known to cause a total reflection of the sound by virtue of a soft-wall condition, for which the radiation in directions nearly parallel to the surface is vanishing (effect known as Lloyd's mirror). The horizontal lobes of the dipole in Fig. 13 would therefore be efficiently extinguished by this effect. The reflection on the water surface is not considered here for conciseness, but it is simply modeled by using the image principle, jointly with the present approach. Yet it is worth noting that such a beneficial effect on a mode requires a half-lobe phasing. If this phasing is imposed on the mode of order n as a result of the synchronization of the propellers, the zero phasing is automatically obtained on the mode of order $2n$, characterized by a twice smaller azimuthal lobe size.

The dramatic effect of asymptotic scattering on a circular distribution of phased stationary sources is understood as follows. Because diffraction is a matter of compared source-to-obstacle distance and frequency, it strongly differs for all angular positions of elementary sources along their circle (thus for various blade-segment positions along their path). This causes imbalance in the partial cancellations which determine the efficiency of a source-mode, hence enhanced noise radiation. This effect is clearly seen in Figs- 13b and 14b. As the cylinder and the propellers are positioned farther from each other, the imbalance is reduced and the sound cancellation becomes more pronounced, leading to less sound. The Helmholtz numbers are $kL = 3.4 \times 10^{-2}$ and $kL = 1.4 \times 10^{-1}$ for the modes $n = 2$ and $n = 3$, respectively. An interesting feature in Fig. 13b is that the area of sound extinction is enlarged in the bottom part of the map. In the same time, the amplification regime is avoided. This increasing-distance effect between the sources and the cylinder could mimic an interesting way to reduce the noise of synchronized propellers near a hull.

The most important outcome of this section is that all higher-order modes n of a pair of contra-rotating source-modes give a negligible free-field radiation, whereas they experience a strong amplification in the compact limit, in the presence of the cylinder. The amplification generates a dipole like pattern. Moreover, higher-order modes must be considered as more compact in the sense that the limit value of kL below which they are amplified increases. The acoustic installation effects are crucial in compact configurations. Finally, the noise of two installed propellers differs significantly from what the free-field noise is, even considering the same sources.
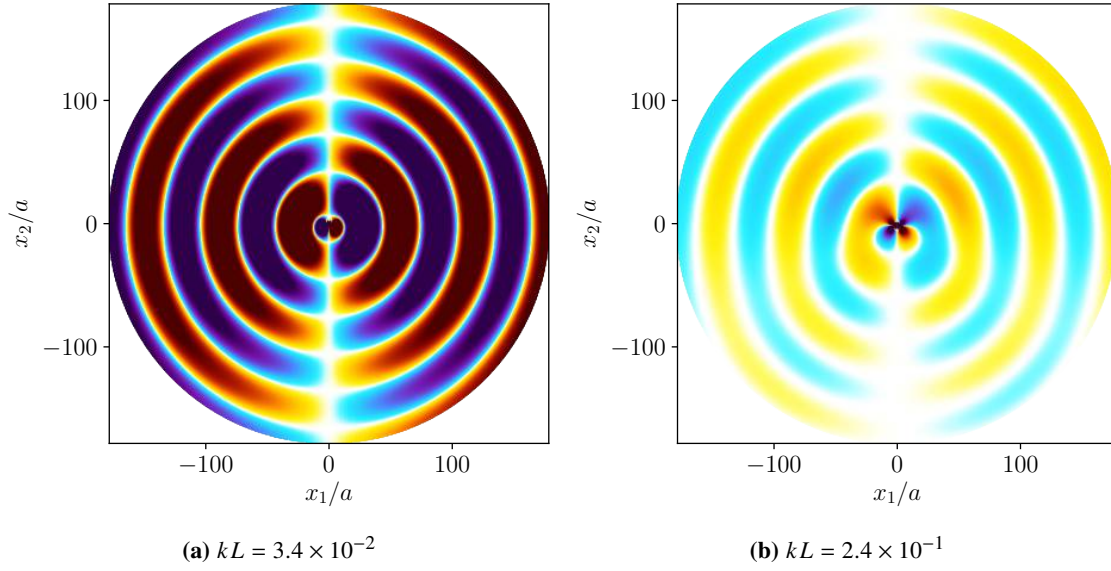
(a) $kL = 3.4 \times 10^{-2}$ **(b)** $kL = 2.4 \times 10^{-1}$

Fig. 13 Instantaneous pressure field maps for the pair of contrarotating source modes in the presence of a scattering cylinder for the modes $n = \pm 2$ at a distance between cylinder to source circle $kL = 3.4 \times 10^{-2}$ (a) and $kL = 2.4 \times 10^{-1}$ (b) . Frequency 10 Hz. Sources are located at an angle of $\theta_c = -\pi/4$ below x-axis. Same color scale on both plots
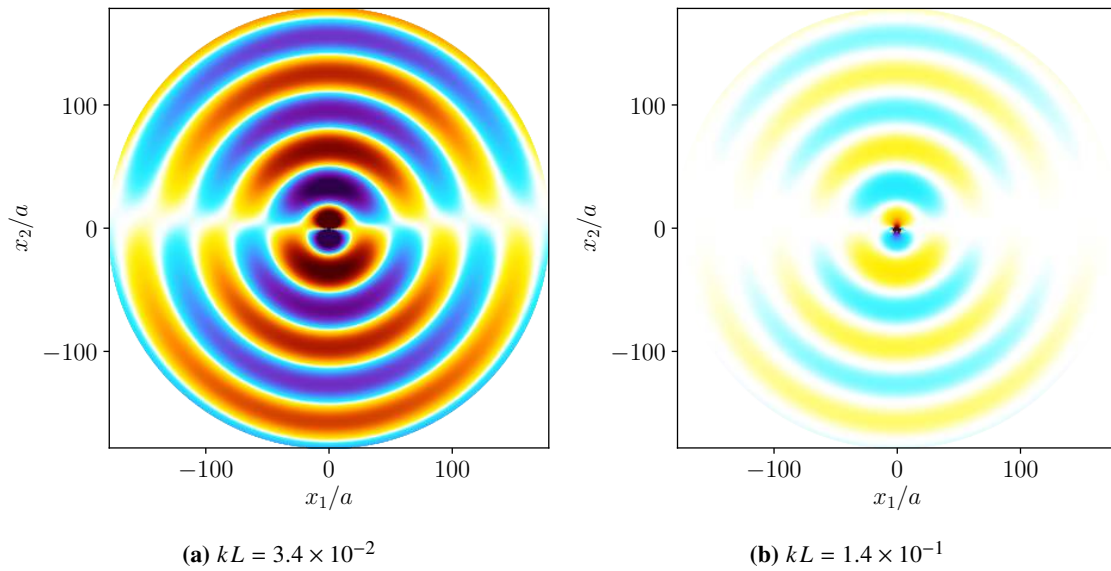
(a) $kL = 3.4 \times 10^{-2}$ **(b)** $kL = 1.4 \times 10^{-1}$

Fig. 14 Instantaneous pressure field maps for the pair of contrarotating source modes in the presence of a scattering cylinder for the modes $n = \pm 3$ at a distance between cylinder to source circle $kL = 3.4 \times 10^{-2}$ (a) and $kL = 1.4 \times 10^{-1}$ (b) . Frequency 10 Hz, center-to-center mode sources distance $d = 5.7 \, R_0$ with $R_0 = 1$ m. Sources are located at an angle of $\theta_c = -\pi/4$ below x-axis. Same color scale on both plots

V. Tailored Green's Function and Source-Mode Radiation in the Asymptotic Regime

The specific parameter ranges of installed marine propellers make the main results expected from an asymptotic analysis, shortly outlined in this section to interpret the exact calculations. The tailored Green's function is developed in its compact regime by using asymptotic forms of Hankel and Bessel functions given by Abramowitz & Stegun [23]. Consider an observer in the acoustic far field and distributed sources over a circle remaining close to the scattering

cylinder, the latter being acoustically compact, so that $kr_x \gg 1$, $kr_y \ll 1$, $ka \ll 1$. The dominant scattered sound pressure radiated by the point dipole in the asymptotic regime for $n > 1$ is obtained by only retaining the leading orders in the derivatives of the Green's function, kr_y and ka being assumed of the same order of magnitude. The detailed derivations will be detailed in another dedicated publication. Only the principle is outlined here. Once the asymptotic form of the scattered field of a single dipole is obtained, the total sound of a source-mode is derived by computing the integral over the source-point angle α. The integral can be expressed analytically. The asymptotic acoustic scattered pressure for two propellers, for $n > 1$ and for half-lobe phasing, is found proportional to:

$$p_s(r_x, \theta_x) \sim \frac{\pi k}{2} n \left(\frac{a}{D}\right)^2 \left(\frac{R_0}{D}\right)^{n-1} \cos(\theta_x) \sqrt{\frac{2}{\pi k r_x}} \, e^{i(kr_x - \pi/4)} \,. \tag{5}$$

The most important feature is that, whatever the order n of the source mode is, the asymptotic scattering by the compact Green's function of the cylinder generates a standing wave. The factor $n(R_0/D)^{n-1}$ only determines the amplitude of the radiated field, decreasing as n increases. With the same level of approximations, the derivatives of the free-field Green's function for $n > 1$ lead to a zero direct sound field, which means that estimating $p_i(r_x, \theta_x)$ would require to pursue the expansion to the nearest higher-order term.

Since the exact Green function is valid for both compact and non compact configurations, the asymptotic form can be used to determine scaling laws. The parameters characteristic of the model can be varied in order to recover the classical diffraction properties. This is reported as an example in Fig 15, where the SPL (Sound Pressure Level) profiles of both the asymptotic form (dashed black lines) and the scattered part of the exact Green's function (plain lines) are plotted as a function of a/R_0, also varying the mode order. The sound pressure level, expressed in arbitrary decibels, is averaged over a circle in the far field for a fixed distance L between cylinder edge and propeller axis ($kL = 3.4 \times 10^{-2}$). Both the exact and asymptotic solutions are found to coincide. The figure also indicates a well-defined maximum for the scattered SPL marked by an asterisk (*), reached at lower values of a/R_0 as the mode order increases. The maximum amplitude is found to also decrease as the mode order increases, for the same assumed dipole strength. Furthermore, the SPL decreases beyond the maximum, more rapidly for higher-order modes. These features characterize the asymptotic regime of diffraction resulting from the compact form of the Green's function. The results could differ for other sets of parameters.
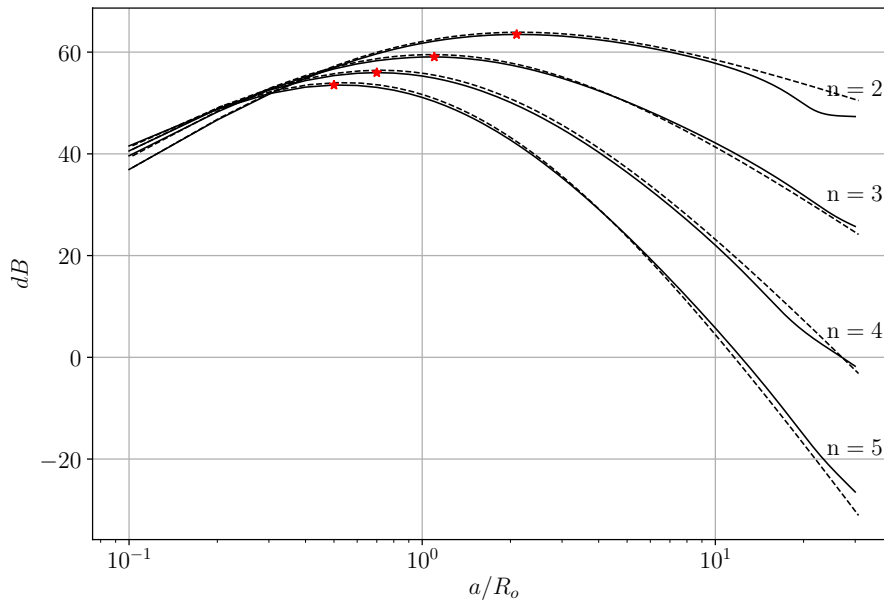
Fig. 15   averaged SPL of the asymptotic form (- - -) and of the exact scattered-field Green's function (—-) for various modes, as functions of a/R_0 at $kL = 3.4 \times 10^{-2}$. Arbitrary decibel scale.

Conclusion

The present work addressed fundamental features of the very-low frequency tonal noise of installed marine propellers, at first multiples of the Blade-Passing Frequency (BPF). Taking account of the extremely low Mach numbers in marine applications and of the very low Helmholtz numbers, based on the size of a domain encompassing the propeller and the cross-section of a scattering hull, two theoretical aspects of the tonal noise deserve attention. Both are related to the fact that the BPF tones are combinations of spinning radiation modes. Firstly, all modes of absolute orders $|n| \geq 2$ are evanescent in free field, because of an equivalent polar order higher than the dipolar order of the elementary constituting sources. Secondly, compact bodies are able to strongly increase the radiation of sources of high polar order placed very close to them, in particular the radiation of the modes. A small-scale experiment has been performed in air with a miniature propeller, in equivalent conditions of Helmholtz number, in order to evidence the amplification of the tonal noise by a rigid scattering cylinder. The first two blade-passing frequencies were observed to be highly contributing to the tonal noise of the propeller. The amplitudes of these tones were found very weak in free field and to increase by typically about 15 dB, once the propeller was approached in the very vicinity of the cylinder. A simple, two-dimensional analytical formulation, based on the Green's function of the rigid cylinder for the Helmholtz equation and on the notion of source-modes, has been implemented, confirming this acoustic installation effect. Though focused on the rotor-locked modes $n = \mu B$ (μ being the BPF order and B the blade number) corresponding to the steady-loading noise and thickness noise, the developments hold for arbitrary mode order. The most spectacular result is that the amplification always generates the radiating mode $n = -1$ for any direct mode of positive order. This modal property was in turn verified in the experiment, by performing a modal expansion of the field measured with a circular microphone array. The main theoretical outcomes have also been reproduced by an asymptotic analysis, developing the tailored Green's function in its compact regime.

In a second step, the analytical model has been used to infer the radiating properties of synchronized contra-rotating source-modes representative of side-by-side marine propellers, combined with the effect of the scattering cylinder. In the asymptotic regime, a resulting equivalent dipole is featured, the axis of which depends on the phasing between the two source-modes. This could be used to balance the aforementioned amplification by taking benefit from the Lloyd's mirror effect. More generally, the proposed model could be used in the future to identify ranges of parameters for which the installation of marine propellers would induce prejudicial effects in terms of noise.

References

[1] Crighton, D., and Leppington, F., "On the scattering of aerodynamic noise," *Journal of Fluids Mechanics*, Vol. 46, 1971, pp. 577–597.

[2] Doak, P., "Acoustic radiation froma turbulent fluid containing foreign bodies," *Proceedings ofthe Royal Society of London*, , No. 254, 1960, pp. 129–145.

[3] Howe, M. S., "Sound generation in a fluid with rigid boundaries," *Acoustics of Fluid–Structures Interactions*, Cambridge, 1998, p. 164–166.

[4] Curle, N., "The influence of solid boundaries upon aerodynamic sound," *Proceedings of the Royal Society of London*, Vol. 231, 1955, pp. 505–514.

[5] Crighton, D., and Leppington, F., "Theory of vortex sound," *Journal of Fluids Mechanics*, Vol. 36, 1964, pp. 177–195.

[6] Williams, J. F., and Hawkings, D., "Sound generation by turbulence and surfaces in arbitrary motion," *Philosophical Transactions of the Royal Society of London*, Vol. A, No. 264, 1969.

[7] FfowcsWilliams, J., and Hawkings, D., "Theory relating to the noise of rotating machinery," *Journal of Sound and Vibration*, Vol. 10, No. (1), 1969, pp. 10–21.

[8] Wei, Y., YangShen, Jin, S., Hub, P., Lan, R., Zhuang, S., and Liu, D., "Scattering effect of submarine hull on propeller non-cavitation noise," *Journal of Sound and Vibration*, Vol. 370, 2016, pp. 319–335.

[9] Testa, C., and Greco, L., "Prediction of submarine scattered noise by the acoustic analogy," *Journal of Sound and Vibration*, Vol. 426, 2018, pp. 186–218.

[10] Farassat, F., "The derivation of a thickness noise formula for the far-field by Isom," *Journal of Sound and Vibration*, Vol. 64, 1979, pp. 159–160.

[11] Isom, M. P., "The Theory of Sound Radiated by a Hovering Transonic Helicopter Blade," *Polytechnic Institute of New York Rept. Poly-AE/AM*, , No. 75-4, 1975.

[12] Goldstein, M., *Aeroacoustics*, McGraw-Hill Book Company, New York, 1976.

[13] Hanson, D. B., and Parzych, D. J., "Theory for noise of propellers in angular in- flow with parametric studies and experimental verificatio," *Final Report United Technologies Corp., Windsor Locks, CT. Standard Div., vol.*, Vol. 1, 1993.

[14] Roger, M., Moreau, S., and Kucukcoskun, K., "On sound scattering by rigid edges and wedges in a flow, with applications to high-lift device aeroacoustics," *Journal of Sound and Vibration*, Vol. 362, 2016, pp. 253–275.

[15] Roger, M., "Near-field fan noise modelling and installation effects due to scattering surfaces," *Fan Noise 2007*, 2007.

[16] Roger, M., and Kucukcoskun, K., "Near-and-far field modeling of advanced tail-rotor noise using source-mode expansions," *Journal of Sound and Vibration*, Vol. 453, 2019, pp. 323–354.

[17] Roger, M., "On combined propeller synchronization and edge scattering for the noise reduction of distributed propulsion systems," 26th *International Congress on Sound and Vibration*, 2019.

[18] Huang, L., "Characterizing computer cooling fan noise," *The Journal of the Acoustical Society of America*, Vol. 114, 2003, pp. 3189–3200.

[19] Huang, L., and Wang, J., "Acoustic analysis of a computer cooling fan," *The Journal of the Acoustical Society of America*, Vol. 118, 2005, pp. 2190–220.

[20] Lu, H. Z., Huang, L., So, R. M. C., and Wang, J. A., "A computational study of the interaction noise from a small axial-flow fan," *The Journal of the Acoustical Society of America*, Vol. 122, 2007, pp. 1404–1415.

[21] Gloerfelt, X., Pérot, F., Bailly, C., and Juvé, D., "Flow-induced cylinder noise formulated as a diffraction problem for low Mach numbers," *Journal of Sound and Vibration*, , No. 287, 2005, pp. 129–151.

[22] Cros, E., Roger, M., and Serre, G., "The radiated field of circular arrays of sources near a scattering cylinder," *Forum acusticum 2020-Lyon*, 2020.

[23] Abramowitz, M., and Stegun, I., *Handbook of mathematical functions*, DOVER, New-York, US, 1970.